

Removal of Hot Saturns in Mass-Radius Plane by Runaway Mass Loss

DANIEL P. THORNGREN,^{1,2} EVE J. LEE,^{3,1} AND ERIC D. LOPEZ^{4,5}

¹*Institute for Research on Exoplanets (iREx), Université de Montréal, Québec, Canada*

²*Department of Physics & Astronomy, Johns Hopkins University, Baltimore, MD, USA*

³*Department of Physics and McGill Space Institute, McGill University, Montréal, Québec, H3A 2T8, Canada*

⁴*NASA Goddard Space Flight Center, 8800 Greenbelt Rd, Greenbelt, MD 20771, USA*

⁵*GSFC Sellers Exoplanet Environments Collaboration*

ABSTRACT

The hot Saturn population exhibits a boundary in mass-radius space, such that no planets are observed at a density less than $\sim 0.1 \text{ g cm}^{-3}$. Yet, planet interior structure models can readily construct such objects as the natural result of radius inflation. Here, we investigate the role XUV-driven mass-loss plays in sculpting the density boundary by constructing interior structure models that include radius inflation, photoevaporative mass loss and a simple prescription of Roche lobe overflow. We demonstrate that planets puffier than $\sim 0.1 \text{ g cm}^{-3}$ experience a runaway mass loss caused by adiabatic radius expansion as the gas layer is stripped away, providing a good explanation of the observed edge in mass-radius space. The process is also visible in the radius-period and mass-period spaces, though smaller, high-bulk-metallicity planets can still survive at short periods, preserving a partial record of the population distribution at formation.

1. INTRODUCTION

Mass loss processes transform large planets into their smaller counterparts and leave imprints in the observed exoplanet population in the shape of deficits. The most famous example is the radius gap that separates the gas-enveloped mini-Neptunes ($\sim 2\text{--}4R_{\oplus}$) from the more rocky super-Earths ($\sim 1\text{--}1.7R_{\oplus}$) which was predicted to exist by theories of photoevaporative mass loss (e.g. Lopez et al. 2012; Owen & Wu 2013) and later confirmed observationally when the host star samples were confined to those that were well-characterized by high-resolution spectra (e.g. Fulton et al. 2017; Fulton & Petigura 2018), asteroseismology (e.g. Van Eylen et al. 2018), or followed up by Gaia and detailed statistical analysis (e.g. Hsu et al. 2019).¹

Another deficit we see in exoplanet population is the sub-Jovian desert, a roughly triangular region in mass-period and radius-period space where we see no Saturn size objects inside orbital periods of a few days, first reported in mass space by Szabó & Kiss (2011)

then in radius space by Beaugé & Nesvorný (2013) and then later confirmed to exist in both mass-period and radius-period spaces by Mazeh et al. (2016). This sub-Jovian desert subsumes the so-called “photoevaporation desert” which refers to the lack of short-period mini-Neptunes whose incident flux would correspond to ~ 650 times that received by the Earth (e.g. Lundkvist et al. 2016), suggesting photoevaporative mass loss to be at play in sculpting at least part of the sub-Jovian desert. Yet another way to view the desert is to consider the orbital period distribution of sub-Saturns ($4\text{--}8R_{\oplus}$). Using a hydrodynamic mass loss model of Kubyshkina et al. (2018), Hallatt & Lee (2022) demonstrated that mass loss alone could reproduce the fall-off in the sub-Saturn occurrence rate at short periods with the stripped Saturns accounting for a fraction of the observed mini-Neptunes and super-Earths.

Although photoevaporation is expected to be an efficient mechanism to strip small planets ($\lesssim 8R_{\oplus}$) of their gaseous envelopes, detailed radiative-hydrodynamic calculations have found that gas giants are resilient against mass loss, losing less than 1% of its total mass over the star’s main-sequence lifetime (e.g. Murray-Clay et al. 2009; Owen & Jackson 2012). It follows that although the lower boundary of the sub-Jovian desert is likely shaped by photoevaporative mass loss, the upper boundary of the desert may require a different explanation.

Valsecchi et al. (2014) proposed that hot Jupiters that are excited onto high enough eccentricities by e.g., Kozai

¹ The same gap is expected to appear prior to mass loss processes purely from the physics of gas accretion (e.g. Lee & Connors 2021; Lee et al. 2022), while subsequent mass loss such as photoevaporation or core-powered envelope mass loss (e.g. Ginzburg et al. 2018; Gupta & Schlichting 2019, 2020) further tune the planet population. Alternatively, the radius gap may not have anything to do with gas envelope and instead stem from two distinct core compositions (e.g. Zeng et al. 2019, but see Aguichine et al. 2021).

can undergo catastrophic Roche lobe overflow and lose all their envelopes, transforming into rocky super-Earths at ultra short periods. While some of the short-period rocky planets may be stripped giants, the lack of strong correlation between the occurrence of ultra-short period planets and the host star metallicity (as opposed to the strong correlation between the occurrence of hot Jupiters and high metallicity of the host star) suggest that this is likely not the main origin channel (Winn et al. 2018).

Instead of mass loss, Matsakos & Königl (2016) considered the boundaries of the desert to be traced by the history of dynamical migration. They proposed that both the upper and the lower boundaries can be reproduced by planets arriving at their closest in orbits by high-eccentricity migration then circularizing onto either the Roche lobe radius or to twice the pericenter distance as expected from secular chaos (Wu & Lithwick 2011). The different shape of the upper and the lower boundary (in the mass-period space) reflects the different mass-radius relationship followed by smaller vs. larger planets. Owen & Lai (2018) combined the expectation from high-eccentricity migration (along with tidal decay) with photoevaporative mass loss and concluded that both mechanisms are required to explain the overall shape with the former being responsible for the upper boundary and the latter being responsible for the lower boundary.

All aforementioned literature relied on their assumed mass-radius relationship for different categories of planets. In this letter, we investigate directly the sub-Jovian population in the radius-mass space and self-consistently compute the evolution of planetary interiors under mass loss. We are motivated by a clean upper boundary in the radius-mass plane that is well-approximated by a constant $\sim 0.1 \text{ g cm}^{-3}$ (see the bottom panel of Figure 1) which also coincides with the region of the parameter space where highly irradiated planets become very large and the mass-radius relationship steepens (Thorngren & Fortney 2018), suggestive of photoevaporative mass loss playing a major role in creating the boundary. By comparison, this density boundary manifests as the very upper edge of the hot Jupiter population in the radius-period space (middle panel) while being coincident with the usual sub-Jovian desert in the mass-period space (top panel).

This paper is organized as follows. In Section 2, we describe how we build time-evolving models of interior structure accounting for XUV-driven mass loss. Our results are presented in Section 3 and we conclude in Section 4.

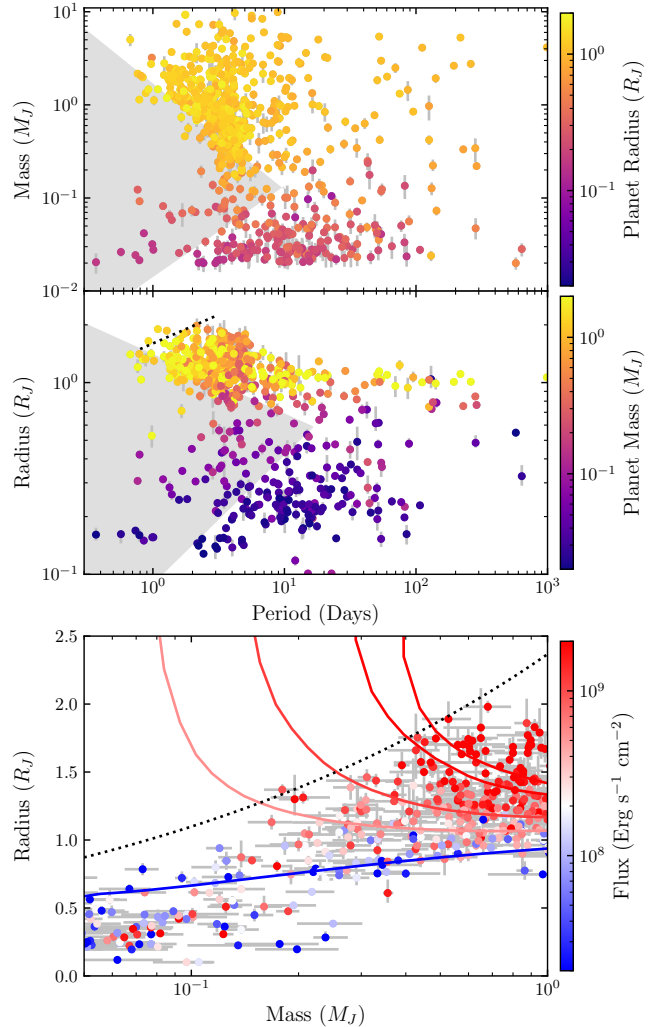


Figure 1. Three views of the observed exoplanet population (our selection criteria are described in Section 2). The top two panels show the conventional view (mass/radius vs. period) of the sub-Jovian desert, which is the shaded area (following Mazeh et al. 2016). We are primarily interested in the low-density boundary seen in mass-radius space (constant 0.1 g cm^{-3} , black dotted line, bottom panel), which is roughly equivalent to the black dotted line in the middle panel and partially overlaps with the mass-period desert. We have also plotted model radius lines (see Section 2) for various incident fluxes demonstrating that planets with density less than 0.1 g cm^{-3} can exist but nevertheless do not in nature.

2. METHODS

We start with gathering data on the observed exoplanets, which we collect from the NASA Exoplanet Archive (DOI: 10.26133/NEA12; Akeson et al. (2013)) and Exoplanet.eu (Schneider et al. 2011). We combine this data and select planets with mass measurements more precise than 30% and radius measurements more precise than 20%. Additionally, we remove those that exhibit any

major data anomalies, e.g. stellar mass differing significantly between observational papers. While we are primarily interested in planets between 0.1 and $1M_J$ and with $a < 0.1$ AU, we include planets outside these ranges for context. It is not our goal to reproduce the absolute abundance of planets and so we do not correct for observational biases. Rather, what is relevant is whether our model is able to account for the *paucity* of planets in spaces where they are favorable to be observed (i.e., large radii and short period).

The majority of our interior structure evolution model is the same as was used in [Thorngren & Fortney \(2019\)](#). These are 1-dimensional models constructed by solving the equations of hydrostatic equilibrium, mass conservation, and an equation of state (EOS):

$$\frac{\partial P}{\partial m} = -\frac{Gm}{4\pi r^4}, \quad (1)$$

$$\frac{\partial r}{\partial m} = \frac{1}{4\pi r^2 \rho}, \quad (2)$$

$$\rho = \rho(P, T), \quad (3)$$

where m and r are the enclosed mass and radii of each layer respectively, P is pressure, ρ is density, T is temperature, and G is the gravitational constant. We use the [Chabrier et al. \(2019\)](#) EOS for a solar-ratio mixture of hydrogen and helium, and a 50-50 mixture of rock and ice for the metals ([Thompson 1990](#)). Metal is distributed in the planet first by building a core up to $15 M_\oplus$, then mixing any remaining metal in the envelope using the additive volumes approximation.

Modelling the thermal evolution of the planet is slightly more complex than in past cases because the mass loss process can also affect the thermal state of the planet. Our model tracks the thermal state of the planet in terms of the envelope specific entropy s , so we seek to calculate its rate of change with time in order to integrate. We start with conservation of total energy E , split into the change in total energy in the core E_c and the change in total energy in the envelope E_e :

$$\frac{dE}{dt} = \frac{dE_c}{dt} + \frac{dE_e}{dt}, \quad (4)$$

where t is time. We assume an isothermal core, and that the core can release energy into the envelope rapidly enough that the core-envelope boundary has no temperature jump. We adopt $c = 7.5 \times 10^6$ erg/g/K (chosen as a typical value for rock, see [Waples & Waples 2004](#)) for the specific heat capacity of the core. The core temperature T_c can then change either because the envelope specific entropy changes or because the envelope loses mass and the core-envelope boundary intersects at a lower pressure and therefore temperature (even at constant entropy). We find that this core depressurization

heat is a negligible effect, but we include it for completeness. The energy change in the envelope is readily calculated from the change in entropy (see e.g. [Thorngren et al. 2016](#)). Putting this all together and solving for the change in entropy with time, we have

$$\frac{dE}{dt} = cM_c \left(\frac{\partial T_c}{\partial M} \frac{\partial M}{\partial t} + \frac{\partial T_c}{\partial s} \frac{\partial s}{\partial t} \right) + \frac{dE_e}{ds} \frac{ds}{dt}; \quad (5)$$

$$\frac{ds}{dt} = \left(\frac{dE}{dt} - cM_c \frac{\partial T_c}{\partial M} \frac{\partial M}{\partial t} \right) / \left(\frac{\partial E_e}{\partial s} + cM_c \frac{\partial T_c}{\partial s} \right), \quad (6)$$

where M is the total mass of the planet, and M_c is the mass of the core. The change in core temperature with mass $\partial T_c / \partial M$ (at constant s) must be calculated by constructing two static models at slightly different envelope masses. Similarly, the denominator of Eq. 6 is computed by constructing two static models of slightly different entropy and evaluating the difference in their energies.

We now consider the energy sources and sinks and equate them Eq. 4:

$$\frac{dE}{dt} = L_{\text{rad}} + \pi R^2 (\epsilon F - 4F_{\text{int}}) \quad (7)$$

where L_{rad} is radioactive heating, R is the radius of the planet, ϵ is the anomalous heating efficiency for which we adopt the median inferred value from [Thorngren & Fortney \(2018\)](#), F is irradiation flux, and F_{int} is the internal cooling flux of the planet. Radioactive heating is computed from the decay of U235, U238, Th232, and K40 following [Nettelmann et al. \(2011\)](#) and [Lopez et al. \(2012\)](#), using [Anders & Grevesse \(1989\)](#) for the radioactive elemental abundances relative to silicon. We find that L_{rad} is an extremely minor component of the energy balance. Finally, F_{int} is calculated for a given envelope specific entropy, surface gravity, and insolation using the non-grey atmosphere models of [Fortney et al. \(2007\)](#).

To model mass-loss, we use the following expression:

$$\dot{M} \approx \frac{\eta \pi F_{XUV} R_{XUV}^3}{GM K_t} \approx \frac{3}{4} \frac{\eta F_{XUV}}{G K_t \rho_{XUV}}; \quad (8)$$

$$K_t = 1 - \frac{3}{2\xi} + \frac{1}{2\xi^3}; \quad (9)$$

$$\xi = \frac{R_{\text{hill}}}{R_{XUV}}, \quad (10)$$

where η is the mass-loss efficiency factor, K_t is a tidal correction factor, R_{hill} is the Hill radius, R_{XUV} is the radius below which the planet becomes opaque to XUV irradiation, which we set at 10 nanobars (a conservative limit of [Lopez et al. 2012](#)), and F_{XUV} is the ex-

treme ultraviolet flux from the parent star which we interpolate from the stellar evolution grid of [Johnstone et al. \(2021\)](#) using the median stellar spin. While Eq. 8 mirrors that of energy-limited approximation from [Watson et al. \(1981\)](#); [Lopez et al. \(2012\)](#); [Lopez & Fortney \(2013\)](#), we do not assume energy-limited mass loss. Instead we use the results of [Caldioli et al. \(2022\)](#), who apply an empirical fitting to a detailed hydrodynamics code ATES ([Caldioli et al. 2021](#)) that encompasses both energy-limited and non-energy-limited regime of mass loss, reported as an effective mass-loss efficiency η that varies non-trivially with incident flux and planetary potential. We find that hot Saturns fall in their low gravity regime where η generally ranges in the few tens of percent.

The deposition depth of XUV irradiation is often quoted as a few nanobars ([Murray-Clay et al. 2009](#); [Caldioli et al. 2021](#)) for giants, although they may be deeper in depending on the mass of the planet ([Owen & Lai 2018](#); [Ionov et al. 2018](#)). We verify that our result is robust to our choice of R_{XUV} between 10 nanobar and 1 microbar. We have rewritten the mass loss rate \dot{M} in terms of ρ_{XUV} the planet bulk density using the XUV radius to highlight the connection between the observed density boundary for hot Saturns (Figure 1) and XUV-driven mass loss.

For planets that grow to overflow their Roche lobes, we assign an arbitrary exponential decay rate of mass with a half-life of 13.8 Myr. We choose this scheme instead of directly modeling the detailed physics of Roche lobe overflow (e.g., [Valsecchi et al. 2014](#)) since the true rate of Roche lobe overflow is fast compared to the lifetime of planets and their thermal evolution, and so these planets would be lost from our hot Saturn population regardless.

3. RESULTS

Fig. 2 illustrates our radius and mass evolution tracks. We show three representative cases for a Saturn-mass planet. At Saturn’s orbit (9.58 AU), the planet experiences no mass loss and cools normally. At 0.07 AU, the planet is a fairly typical hot Saturn, which cools to an inflated equilibrium where the luminosity equals the anomalous heating (see e.g. [Thorngren et al. 2021](#)). The planet experiences modest mass loss over the course of its lifetime.

Placing a Saturn at 0.05 AU has a very different outcome. Although the planet does not initially overflow its Roche lobe nor is the initial mass-loss rate particularly high, the slow erosion of mass accelerates into the catastrophic removal of the envelope at ~ 100 Myrs. This run-away mass loss is effected by an adiabatic expansion of the planet as it enlarges while losing mass

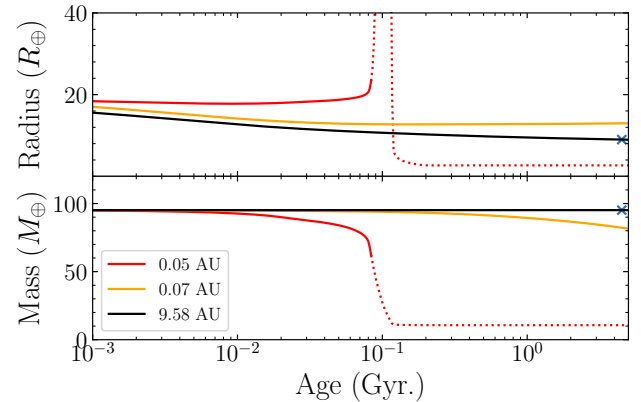


Figure 2. The thermal and mass evolution of a Saturn-mass planet at various semimajor axes. The planet bulk metallicity was tuned to $Z_p = .225$ to match Saturn’s radius (blue x) at 4.5 Gyr and 9.58 AU. If instead placed at 0.07 AU, the planet experiences modest mass-loss over Gyr timescales, but the radius is mostly unchanged. At 0.05 AU, the planet loses mass at increasing rates until the runaway mass-loss strips the envelope from the planet. We have dotted the line after the planet reaches $2.2R_J$ to note that the exact rate of mass-loss post runaway and the final state of the planet depend on the assumed loss rate by Roche lobe overflow and the imposed mass of the core (see Sections 2 and 4). We emphasize that the occurrence of runaway mass-loss is robust.

at constant specific entropy. Critically, the rate of mass loss scales as the radius cubed (recall Eq. 8), enhanced further by the tidal factor K_t . Furthermore, at very low densities the mass-radius relationship becomes particularly steep (see Fig. 1). The result is a positive feedback loop that reaches a head at around 100 Myr, when the planet grows in size rapidly, overflows its Roche lobe, and ejects its envelope, leaving only a stripped core behind. Testing the robustness of this result, we found that even restricting the model radius to $< 2.2R_J$ (roughly the largest planets observed) makes little difference—runaway mass-loss occurs regardless.

Our result of runaway mass loss is reminiscent of what was reported by [Kurokawa & Nakamoto \(2014\)](#) which has since then been criticized for their use of fixed η and overestimating the mass loss rate by fixing the pressure at the bottom of the photoevaporative flow at 1 nanobar ([Owen & Lai 2018](#); [Ionov et al. 2018](#)). The latter authors did not find any evidence of runaway mass loss. Our calculations rigorously account for the variable η and we find that our results are robust to smaller R_{XUV} down to 1 microbar. One of the key reasons why we recover this catastrophic erosion is because we account for the anomalous heating throughout the planet’s thermal evolution instead of at the very end, which keeps our planets puffy. We have verified that when this anoma-

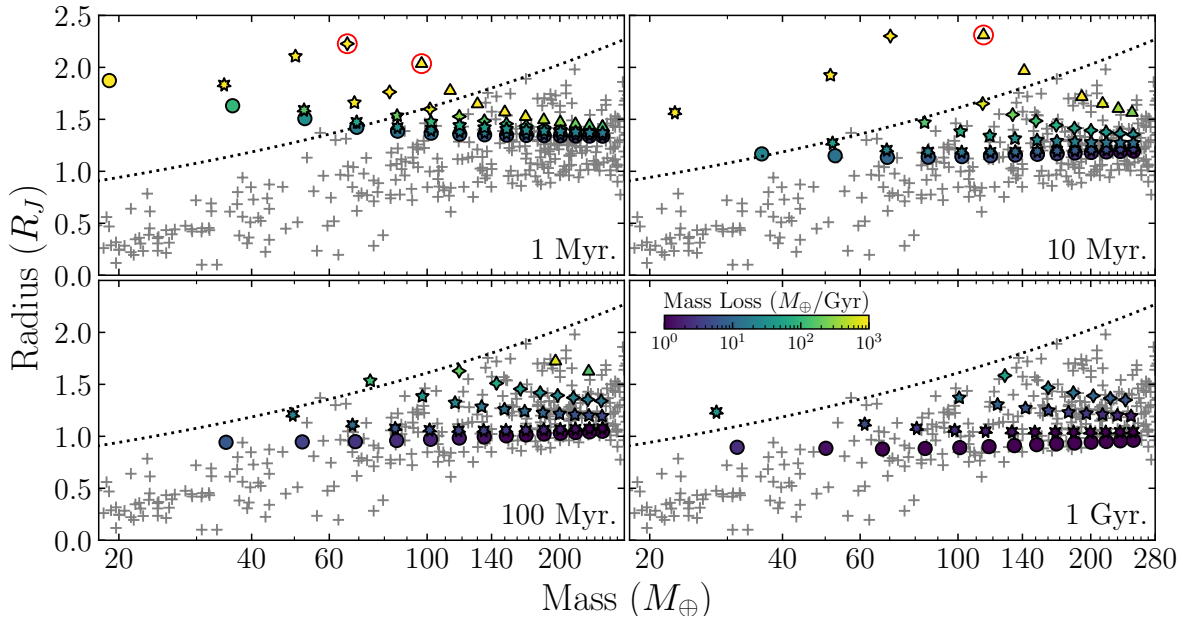


Figure 3. A grid of planets over a range of masses and semi-major axes undergoing mass loss and thermal evolution, color-coded with respect to their rate of mass loss, and different symbols corresponding to semimajor axes (triangles to circles representing 0.03, 0.04, 0.05, 0.07, and 0.1 AU). Planets circled in red have overflowed their Roche lobes. Observed exoplanets are plotted beneath in grey, with the constant density 0.1 g cm^{-3} boundary shown as a dotted line. Runaway mass loss rapidly strips low-density planets down to their cores so that within $\sim 100 \text{ Myr}$, the region above the density boundary is clear of planets. Some additional planets near the boundary continue to lose mass, and a few undergo runaway mass loss later on (for example, the one model planet above the density boundary at 1 Gyr will be lost within the next $\sim 0.5 \text{ Gyr}$).

lous heating is set to zero, the mass loss never reaches a runaway state.

3.1. Carving out the Edges

We are particularly interested in determining the overall effect of mass loss, especially the runaway variety, on the hot Saturn population, irrespective of particular initial distribution of host Saturns arising from planet formation, which is outside the scope of this paper. Instead, we seek to answer the more narrow question: if a hot Saturn of some mass is placed at a particular semi-major axis, can it survive?

We have run our mass loss model on a grid of masses and semimajor axes. The masses were 15 values log-uniformly spaced from $20M_{\oplus}$ to $250M_{\oplus}$ and the semi-major axes were 0.03, 0.04, 0.05, 0.07, and 0.1 AU. The results are shown for several slices in time on Fig. 3 – an animation is also available. We assume a solar-mass star with a median amount of XUV irradiation (i.e., median spin) for its age. Planets on short orbits experience more anomalous heating and consequently maintain a larger radius than those at longer periods after they cool. Short-period, low-density planets are particularly susceptible to runaway mass loss and we observe a clear boundary at $\sim 1 \text{ g cm}^{-3}$ within ~ 100

Myr which persists to $\sim 1 \text{ Gyr}$, matching the observed density boundary of hot Saturns in radius-mass space.

We have also considered the effect of stellar mass, the planet metallicity, and the effective XUV flux on the mass loss rates (Fig. 4). More massive stars have higher bolometric and XUV luminosities so planets around them are more inflated for a given mass and given orbital distance and therefore more susceptible to mass loss. The net result is that the closest-in planets (0.03 AU, triangle points) around higher mass stars lose their envelopes and lose their hot Saturn status while those at longer orbital distances survive against mass loss but stay puffy. Similarly, planets of lower bulk metallicity also appear puffy (due to their lower densities) and so the closest-in planets are lost to mass loss (note the lack of triangle points in the bottom center panel). Those at wider separations are stable against mass loss but will be larger than planets of higher bulk metallicity.

In Figure 3, we see excess of planets of mass $\gtrsim 140M_{\oplus}$ with radii above $1.5 R_J$ in the observations compared to our fiducial model. Our parameter study (Figure 4) suggests that such planets are likely around more massive stars and/or they have lower bulk metallicity. Indeed, planets in our sample above $1.5 R_J$ all orbit around stars more massive than the Sun, with an average mass of 1.41

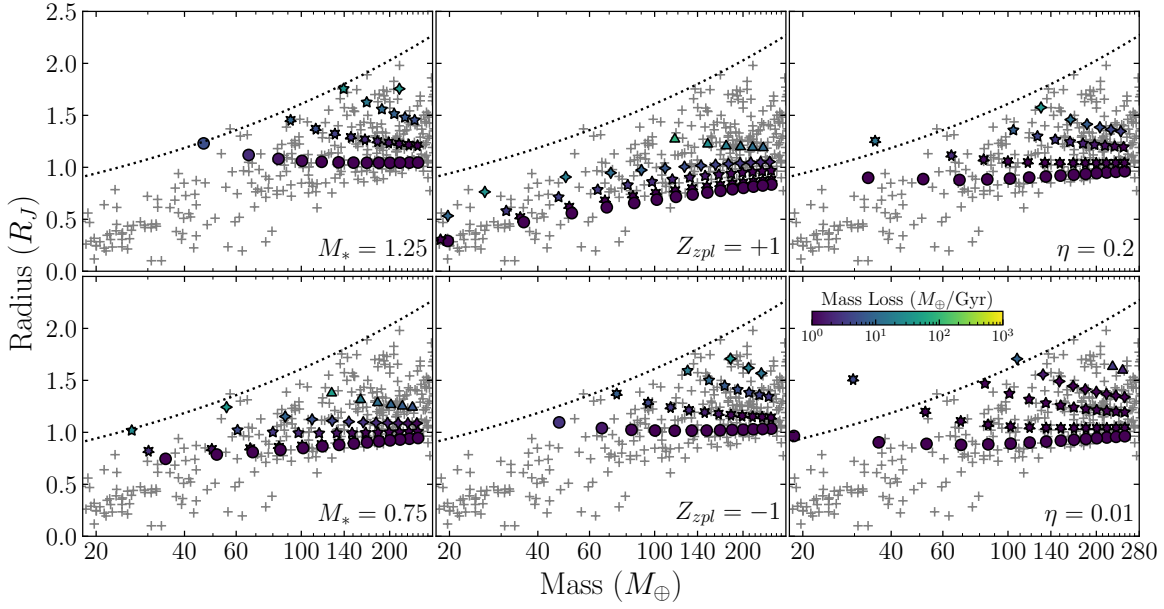


Figure 4. The model planets at 1 Gyr, varying the stellar mass (left), bulk metallicity (center), and XUV mass loss efficiency (right), color-coded with respect to the rate of mass loss. Symbols and the dotted line follow the convention of Figure 3. For the metallicity Z_{pl} , we take the $\pm 1\sigma$ value away from the mean of the mass-metallicity distribution reported by [Thorngren & Fortney \(2018\)](#). This range is broad; for example, a Saturn-mass planet with -1σ metallicity has $15M_{\oplus}$ of metal, whereas at $+1\sigma$ it has $50M_{\oplus}$. With all else equal, planets appear larger around more massive (and brighter) parent stars or for those with low bulk metallicity. These planets are more susceptible to mass loss and so the closest-in planets (triangles) are lost by 1 Gyr. At larger orbital distances, these puffer planets still survive owing to lower XUV flux and fill up the high mass ($\gtrsim 140M_{\oplus}$) and large radii ($\gtrsim 1.5R_J$). The right column shows that our results are only modestly sensitive to mass-loss efficiency with the region to the left of the density boundary being largely vacated between low and high η .

M_{\odot} (vs. $\sim 1.1M_{\odot}$ for $1R_J < R < 1.5R_J$), corroborating our results.

The right panels of Fig. 4 illustrate the effect of varying η . As expected, closest-in planets are lost for higher fixed mass loss efficiency (note the lack of triangle points in the top right panel). Even at a low $\eta=0.01$, the low-density desert is largely cleared out by 1 Gyr, demonstrating that $\sim 0.1\text{g cm}^{-3}$ is the boundary for a runaway mass loss (i.e., when the planet enters the runaway phase, they will be stripped of their sub-Saturn status regardless of the details of how they arrived to such a boundary).

We now explore how the runaway mass loss manifests in the mass-period and radius-period spaces. First, we draw 400 sets of mass, semimajor axis, stellar mass, and metallicity, distributed log-uniformly from 20 to $250M_{\oplus}$ in mass, uniformly from 0.8 to $1.2 M_{\odot}$ in stellar mass, log-uniformly from 0.03 AU to 0.1 AU in semimajor-axis, and the metallicity according to the mass-metallicity relation ([Thorngren et al. 2021](#)). These planets are evolved out to 5 Gyr and the results are shown in Fig. 5. We observe that most of the low-mass, short-period planets have large radii and are quickly

reduced to stripped cores. All model planets near or above $2R_J$ are destroyed by runaway inflation within 100 Myr, shaping the upper edge of the radius distribution. Over 5 Gyr, the sub-Jovian desert in mass-period space is largely carved out by mass loss although it is not fully cleared, mostly due to high-bulk metallicity planets which have small radii, suggesting the formation of hot Saturns disfavors those with high densities. In some cases, tidal inspiral may lead to runaway mass loss, though careful calculation would be needed to examine this possibility as the XUV luminosity will have dropped significantly on inspiral timescales ($\sim \text{Gyr}$).

From our simple initial random distribution of planets, we find that the ones that survive against mass loss to fill in the sub-Jovian desert in mass-period and radius-period spaces are those that have high bulk metallicity (and so higher density). Our result agrees with the discovery of dense Neptune to Saturn size planets found within the desert such as LTT 9799 b ([Jenkins et al. 2020](#)) and TOI-849 b ([Armstrong et al. 2020](#)), although these two planets could also be stripped massive cores of even larger giants.

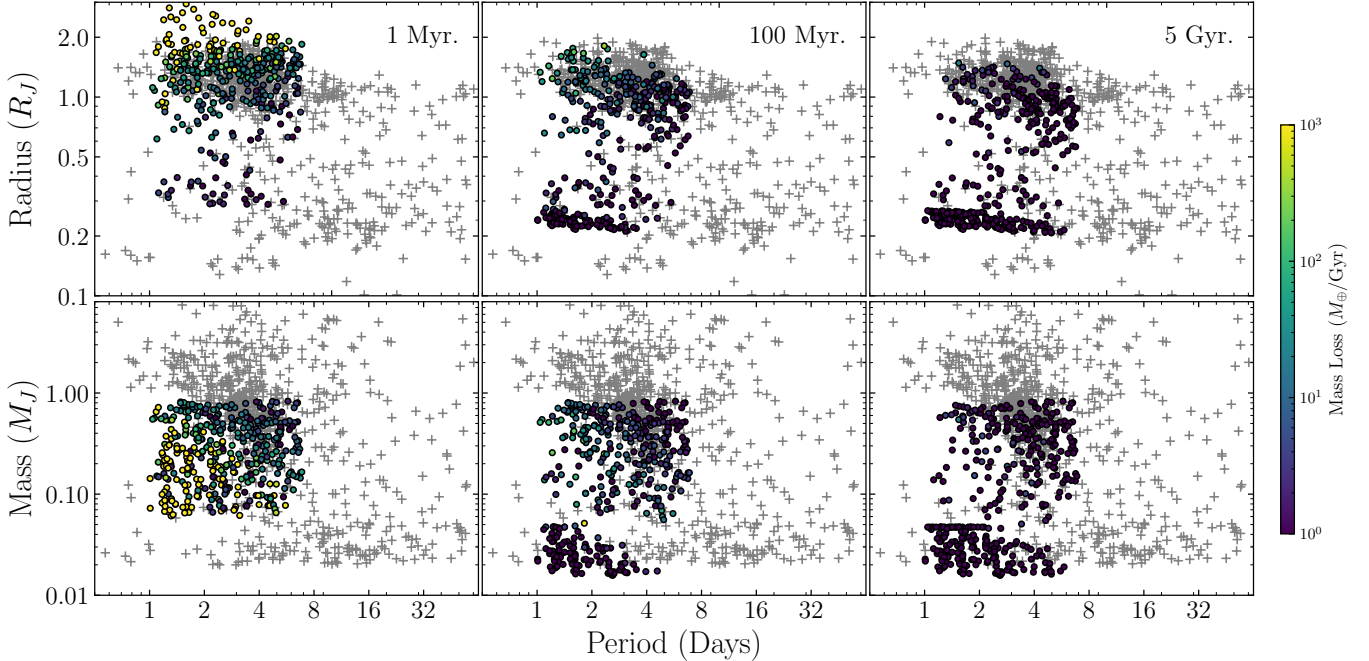


Figure 5. Model planets with random initial properties, plotted as radius against period (top) and mass against period (bottom) at 1 Myr, 100 Myr, and 5 Gyr. The color indicates the rate of mass loss, and the observed population is plotted in grey. In radius-period space, runaway mass loss curves out the upper edge of the radius distribution, removing the planets $\gtrsim 2R_J$ from 1 Myr transforming them to $\lesssim 0.3R_J$ by 5 Gyr. In mass-period space, runaway mass loss removes the lower left half of the triangle (the yellow points) at 1 Myr and vacate that region by 5 Gyr, transforming them into $\lesssim 0.04M_J$ planets.

4. DISCUSSION AND CONCLUSION

Our primary conclusion is that hot Saturns can undergo runaway mass loss caused by positive feedback between the adiabatic expansion of the radius and the mass loss (Fig. 2). In many cases, this leads to Roche lobe overflow, though this is not necessary to remove the planets’ envelope. Over a range of stellar masses, planet bulk metallicity, and the XUV mass loss efficiency, we find that this process can robustly sculpt the low density boundary at $\sim 0.1 \text{ g cm}^{-3}$ (Figs. 3 and 4).

In radius-period space, the radii for our initial distribution already show a relative paucity of planets at $\sim 0.3\text{--}1.0R_J$ inside ~ 3 days, similar to what is observed. This initial radius-period paucity arises from a sudden rise in radius over a small dynamic range in mass at high incident flux (see the model mass-radius relation curves in the bottom panel of Figure 1). Subsequent XUV-driven mass-loss quickly removes planets from the sub-Jovian desert in mass-period space, though somewhat too many planets appear to remain in the desert compared to the observations (Fig. 5). To completely clear out the desert, we may need to more carefully account for Roche lobe overflow and tidal processes (e.g. Valsecchi et al. 2015) in our models, but perhaps more important is the relatively simple choice of input distribution, especially on planet mass and period. For

example, Hallatt & Lee (2022) were able to reproduce the desert (in terms of the decline in sub-Saturn occurrence rate at short periods) through XUV-driven mass-loss and a careful consideration of the initial core mass function and gas accretion theory.

Planets that lose their envelopes collect around ~ 0.2 to $\sim 0.3 R_J$ based on their initial core mass, which we imposed in Section 2. This assumption does not change the triggering of runaway mass-loss, but it does impact the final state. This suggests that if we are able to identify probable stripped cores, they would be a unique window into the deep interiors of giant planets. A few such candidates have already been proposed (Petigura et al. 2017; Jenkins et al. 2020; Armstrong et al. 2020), and a targeted study would likely identify more.

Our results differ somewhat from Owen & Lai (2018) and Ionov et al. (2018), who argue that photoevaporative mass loss is unable to explain the upper edge of the sub-Jovian desert (i.e., hot Saturns are resilient against mass loss). First, we argue that the effect of mass loss is more clearly seen in radius-mass space rather than mass-period or radius-period. Second, and more importantly, we include the anomalous heating of hot giants found in Thorngren & Fortney (2018) throughout the planets’ evolution, resulting in larger planets more vulnerable to mass loss than Owen & Lai (2018), who evolve

their planets without heating and then inflate them after mass-loss has completed. We believe our approach is more consistent with the observations, as in [Thorngrén et al. \(2021\)](#), it was found that young planets are as large or larger than their older equivalents once the present-day incident flux is controlled for.

Recently, [Vissapragada et al. \(2022\)](#) examined a set of seven transiting planets on the (mostly upper) edge of the desert in mass-period space. They found that none of the planets were undergoing massive mass loss despite sizable XUV fluxes. We do not find their result to be in tension with ours as all the planets they investigated have densities larger than the 0.1 g cm^{-3} boundary, ranging from 0.172 to 0.717 g cm^{-3} . The lowest density planet, WASP-177 b is still interesting as a planet near the density edge, but they find that its mass loss rate is quite low, which could be due to its old age of ~ 10 Gyr ([Turner et al. 2019](#)), as XUV luminosity declines as the star ages.

Future work on this area could investigate the potential mass-loss histories of giant planets near the low-density boundary. One good candidate for this is WASP-17 b ([Anderson et al. 2010](#)), the largest known planet with a well-determined mass and radius, and one which is likely to be losing mass at a prodigious rate. Qatar-10 b ([Alsubai et al. 2019](#)) and WASP-76 b ([West et al. 2016](#)) are also good cases for substantial

ongoing mass loss. Also of interest are the smaller and lower-mass planets which are nevertheless near the 0.1 g cm^{-3} boundary, including WASP-20 A b ([Anderson et al. 2015](#)) and WASP-153 b ([Demangeon et al. 2018](#)). While these planets are not experiencing runaway mass-loss at the present day, they likely are experiencing some loss, and they may be nearing runaway. Measuring both the mass loss rates and XUV fluxes of their parent stars could help to pinpoint some of the fine details of this process.

ACKNOWLEDGMENTS

We thank Jonathan Fortney and Ruth Murray-Clay for helpful discussions. D.P.T. thanks the Institute for Research on Exoplanets (iREx) for support via the Trotter Fellowship and Johns Hopkins University for support via the Davis Fellowship. E.J.L. gratefully acknowledges support from NSERC, FRQNT, the McGill Space Institute, and the William Dawson Scholarship from McGill. E.D.L. would like to acknowledge support from the GSFC Sellers Exoplanet Environments Collaboration (SEEC), which is funded in part by the NASA Planetary Science Division’s Internal Scientist Funding Model.

REFERENCES

- Aguichine, A., Mousis, O., Deleuil, M., & Marcq, E. 2021, *The Astrophysical Journal*, 914, 84, doi: [10.3847/1538-4357/abfa99](#)
- Akeson, R. L., Chen, X., Ciardi, D., et al. 2013, *Publications of the Astronomical Society of the Pacific*, 125, 989, doi: [10.1086/672273](#)
- Alsubai, K., Tsvetanov, Z. I., Pyrzas, S., et al. 2019, *The Astronomical Journal*, 157, 224, doi: [10.3847/1538-3881/ab19bc](#)
- Anders, E., & Grevesse, N. 1989, *Geochimica et Cosmochimica Acta*, 53, 197, doi: [10.1016/0016-7037\(89\)90286-X](#)
- Anderson, D. R., Hellier, C., Gillon, M., et al. 2010, *The Astrophysical Journal*, 709, 159, doi: [10.1088/0004-637X/709/1/159](#)
- Anderson, D. R., Collier Cameron, A., Hellier, C., et al. 2015, *Astronomy and Astrophysics*, 575, A61, doi: [10.1051/0004-6361/201423591](#)
- Armstrong, D. J., Lopez, T. A., Adibekyan, V., et al. 2020, *Nature*, 583, 39, doi: [10.1038/s41586-020-2421-7](#)
- Beaugé, C., & Nesvorný, D. 2013, *The Astrophysical Journal*, 763, 12, doi: [10.1088/0004-637X/763/1/12](#)
- Caldirolì, A., Haardt, F., Gallo, E., et al. 2021, *Astronomy and Astrophysics*, 655, A30, doi: [10.1051/0004-6361/202141497](#)
- . 2022, *Astronomy and Astrophysics*, 663, A122, doi: [10.1051/0004-6361/202142763](#)
- Chabrier, G., Mazevet, S., & Soubiran, F. 2019, *The Astrophysical Journal*, 872, 51, doi: [10.3847/1538-4357/aaf99f](#)
- Demangeon, O. D. S., Faedi, F., Hébrard, G., et al. 2018, *Astronomy and Astrophysics*, 610, A63, doi: [10.1051/0004-6361/201731735](#)
- Fortney, J. J., Marley, M. S., & Barnes, J. W. 2007, *The Astrophysical Journal*, 659, 1661, doi: [10.1086/512120](#)
- Fulton, B. J., & Petigura, E. A. 2018, *The Astronomical Journal*, 156, 264, doi: [10.3847/1538-3881/aae828](#)
- Fulton, B. J., Petigura, E. A., Howard, A. W., et al. 2017, *The Astronomical Journal*, 154, 109, doi: [10.3847/1538-3881/aa80eb](#)
- Ginzburg, S., Schlichting, H. E., & Sari, R. 2018, *Monthly Notices of the Royal Astronomical Society*, 476, 759, doi: [10.1093/mnras/sty290](#)

- Gupta, A., & Schlichting, H. E. 2019, *Monthly Notices of the Royal Astronomical Society*, 487, 24, doi: [10.1093/mnras/stz1230](https://doi.org/10.1093/mnras/stz1230)
- . 2020, *Monthly Notices of the Royal Astronomical Society*, 493, 792, doi: [10.1093/mnras/staa315](https://doi.org/10.1093/mnras/staa315)
- Hallatt, T., & Lee, E. J. 2022, *The Astrophysical Journal*, 924, 9, doi: [10.3847/1538-4357/ac32c9](https://doi.org/10.3847/1538-4357/ac32c9)
- Hsu, D. C., Ford, E. B., Ragozzine, D., & Ashby, K. 2019, *The Astronomical Journal*, 158, 109, doi: [10.3847/1538-3881/ab31ab](https://doi.org/10.3847/1538-3881/ab31ab)
- Ionov, D. E., Pavlyuchenkov, Y. N., & Shematovich, V. I. 2018, *Monthly Notices of the Royal Astronomical Society*, 476, 5639, doi: [10.1093/mnras/sty626](https://doi.org/10.1093/mnras/sty626)
- Jenkins, J. S., Díaz, M. R., Kurtovic, N. T., et al. 2020, *Nature Astronomy*, 4, 1148, doi: [10.1038/s41550-020-1142-z](https://doi.org/10.1038/s41550-020-1142-z)
- Johnstone, C. P., Bartel, M., & Güdel, M. 2021, *Astronomy and Astrophysics*, 649, A96, doi: [10.1051/0004-6361/202038407](https://doi.org/10.1051/0004-6361/202038407)
- Kubyskhina, D., Fossati, L., Erkaev, N. V., et al. 2018, *The Astrophysical Journal*, 866, L18, doi: [10.3847/2041-8213/aae586](https://doi.org/10.3847/2041-8213/aae586)
- Kurokawa, H., & Nakamoto, T. 2014, *The Astrophysical Journal*, 783, 54, doi: [10.1088/0004-637X/783/1/54](https://doi.org/10.1088/0004-637X/783/1/54)
- Lee, E. J., & Connors, N. J. 2021, *The Astrophysical Journal*, 908, 32, doi: [10.3847/1538-4357/abd6c7](https://doi.org/10.3847/1538-4357/abd6c7)
- Lee, E. J., Karalis, A., & Thorngren, D. P. 2022, *Creating the Radius Gap without Mass Loss*, arXiv, doi: [10.48550/arXiv.2201.09898](https://doi.org/10.48550/arXiv.2201.09898)
- Lopez, E. D., & Fortney, J. J. 2013, *The Astrophysical Journal*, 776, 2, doi: [10.1088/0004-637X/776/1/2](https://doi.org/10.1088/0004-637X/776/1/2)
- Lopez, E. D., Fortney, J. J., & Miller, N. 2012, *The Astrophysical Journal*, 761, 59, doi: [10.1088/0004-637X/761/1/59](https://doi.org/10.1088/0004-637X/761/1/59)
- Lundkvist, M. S., Kjeldsen, H., Albrecht, S., et al. 2016, *Nature Communications*, 7, 11201, doi: [10.1038/ncomms11201](https://doi.org/10.1038/ncomms11201)
- Matsakos, T., & Königl, A. 2016, *The Astrophysical Journal*, 820, L8, doi: [10.3847/2041-8205/820/1/L8](https://doi.org/10.3847/2041-8205/820/1/L8)
- Mazeh, T., Holczer, T., & Faigler, S. 2016, *Astronomy & Astrophysics*, 589, A75, doi: [10.1051/0004-6361/201528065](https://doi.org/10.1051/0004-6361/201528065)
- Murray-Clay, R. A., Chiang, E. I., & Murray, N. 2009, *The Astrophysical Journal*, 693, 23, doi: [10.1088/0004-637X/693/1/23](https://doi.org/10.1088/0004-637X/693/1/23)
- Nettelmann, N., Fortney, J. J., Kramm, U., & Redmer, R. 2011, *The Astrophysical Journal*, 733, 2, doi: [10.1088/0004-637X/733/1/2](https://doi.org/10.1088/0004-637X/733/1/2)
- Owen, J. E., & Jackson, A. P. 2012, *Monthly Notices of the Royal Astronomical Society*, 425, 2931, doi: [10.1111/j.1365-2966.2012.21481.x](https://doi.org/10.1111/j.1365-2966.2012.21481.x)
- Owen, J. E., & Lai, D. 2018, *Monthly Notices of the Royal Astronomical Society*, 479, 5012, doi: [10.1093/mnras/sty1760](https://doi.org/10.1093/mnras/sty1760)
- Owen, J. E., & Wu, Y. 2013, *The Astrophysical Journal*, 775, 105, doi: [10.1088/0004-637X/775/2/105](https://doi.org/10.1088/0004-637X/775/2/105)
- Petigura, E. A., Sinukoff, E., Lopez, E. D., et al. 2017, *The Astronomical Journal*, 153, 142, doi: [10.3847/1538-3881/aa5ea5](https://doi.org/10.3847/1538-3881/aa5ea5)
- Schneider, J., Dedieu, C., Le Sidaner, P., Savalle, R., & Zolotukhin, I. 2011, *Astronomy and Astrophysics*, 532, A79, doi: [10.1051/0004-6361/201116713](https://doi.org/10.1051/0004-6361/201116713)
- Szabó, G. M., & Kiss, L. L. 2011, *The Astrophysical Journal Letters*, 727, L44, doi: [10.1088/2041-8205/727/2/L44](https://doi.org/10.1088/2041-8205/727/2/L44)
- Thompson, S. L. 1990, *ANEOS Analytic Equations of State for Shock Physics Codes Input Manual*, Tech. Rep. SAND-89-2951, 6939284, Sandia National Laboratory, doi: [10.2172/6939284](https://doi.org/10.2172/6939284)
- Thorngren, D., & Fortney, J. J. 2019, *The Astrophysical Journal*, 874, L31, doi: [10.3847/2041-8213/ab1137](https://doi.org/10.3847/2041-8213/ab1137)
- Thorngren, D. P., & Fortney, J. J. 2018, *The Astronomical Journal*, 155, 214, doi: [10.3847/1538-3881/aaba13](https://doi.org/10.3847/1538-3881/aaba13)
- Thorngren, D. P., Fortney, J. J., Lopez, E. D., Berger, T. A., & Huber, D. 2021, *The Astrophysical Journal*, 909, L16, doi: [10.3847/2041-8213/abe86d](https://doi.org/10.3847/2041-8213/abe86d)
- Thorngren, D. P., Fortney, J. J., Murray-Clay, R. A., & Lopez, E. D. 2016, *The Astrophysical Journal*, 831, 64, doi: [10.3847/0004-637X/831/1/64](https://doi.org/10.3847/0004-637X/831/1/64)
- Turner, O. D., Anderson, D. R., Barkaoui, K., et al. 2019, *Monthly Notices of the Royal Astronomical Society*, doi: [10.1093/mnras/stz742](https://doi.org/10.1093/mnras/stz742)
- Valsecchi, F., Rappaport, S., Rasio, F. A., Marchant, P., & Rogers, L. A. 2015, *The Astrophysical Journal*, 813, 101, doi: [10.1088/0004-637X/813/2/101](https://doi.org/10.1088/0004-637X/813/2/101)
- Valsecchi, F., Rasio, F. A., & Steffen, J. H. 2014, *The Astrophysical Journal*, 793, L3, doi: [10.1088/2041-8205/793/1/L3](https://doi.org/10.1088/2041-8205/793/1/L3)
- Van Eylen, V., Agentoft, C., Lundkvist, M. S., et al. 2018, *Monthly Notices of the Royal Astronomical Society*, 479, 4786, doi: [10.1093/mnras/sty1783](https://doi.org/10.1093/mnras/sty1783)
- Vissapragada, S., Knutson, H. A., Greklek-McKeon, M., et al. 2022, *The Astronomical Journal*, 164, 234, doi: [10.3847/1538-3881/ac92f2](https://doi.org/10.3847/1538-3881/ac92f2)
- Waples, D., & Waples, J. 2004, *Natural Resources Research*, 13, 97, doi: [10.1023/B:NARR.0000032647.41046.e7](https://doi.org/10.1023/B:NARR.0000032647.41046.e7)
- Watson, A. J., Donahue, T. M., & Walker, J. C. G. 1981, *Icarus*, 48, 150, doi: [10.1016/0019-1035\(81\)90101-9](https://doi.org/10.1016/0019-1035(81)90101-9)

West, R. G., Hellier, C., Almenara, J.-M., et al. 2016,

Astronomy & Astrophysics, 585, A126,

doi: [10.1051/0004-6361/201527276](https://doi.org/10.1051/0004-6361/201527276)

Winn, J. N., Sanchis-Ojeda, R., & Rappaport, S. 2018, New
Astronomy Reviews, 83, 37,
doi: [10.1016/j.newar.2019.03.006](https://doi.org/10.1016/j.newar.2019.03.006)
Wu, Y., & Lithwick, Y. 2011, The Astrophysical Journal,
735, 109, doi: [10.1088/0004-637X/735/2/109](https://doi.org/10.1088/0004-637X/735/2/109)
Zeng, L., Jacobsen, S. B., Sasselov, D. D., et al. 2019,
Proceedings of the National Academy of Science, 116,
9723, doi: [10.1073/pnas.1812905116](https://doi.org/10.1073/pnas.1812905116)